SAND2014-3674C

Quantification of image registration error

Adoum H. Mahamat, Eric A. Shields

Sandia National Laboratories, Albuquerque, NM 87185

ABSTRACT

Image registration is a digital image processing technique that takes two or more of images of a scene in different-coordinate systems and transforms them into a single coordinate system. Image registration is a necessary step in many advanced image processing techniques, such as multi-frame super-resolution. For that reason, registration accuracy is very crucial. While image registration is usually performed on intensity images, one can perform the registration using metric images as well. This paper will present registration methods and their accuracies for various noise levels for the case of pure translational image motion. Registration techniques will be applied to the images themselves as well as to phase congruency images, gradient images, and edge-detected images. This study will also investigate registration of under-sampled images. Noise-free images are degraded using three types of noise: additive Gaussian noise, fixed-pattern noise along the column direction, and a combination of these two. The registration error is quantified for two registration algorithms with three different images as a function of the signal-to-noise ratio. A test on the usefulness of the registration and registration accuracy is done on the intensity images of the Stokes imaging polarimeter.

Keywords: Super-resolution, image registration, metric registration, Stokes polarimetric,

INTRODUCTION

Image registration is used in many fields where image processing has a great importance. Such fields include remote sensing, medical imaging, and polarization imaging. In all those imaging fields, several image frames of the same scene are taken and analyzed together to extract information. Many of these algorithms require images to be registered to each other before processing. We present the results of a study of two registration algorithms with three different images to determine their registration errors for different signal-to-noise ratios. In addition to the signal-to-noise (SNR) ratio variations, three different noises were added to the noise-free images before registration.

The first registration algorithm is based on the registration technique implemented by *Sicairos et al*[1]. This registration algorithm obtains an initial estimate of the cross-correlation peak via the fast Fourier transform (FFT) and then refines the shift estimation by up sampling the discrete Fourier transform (DFT) only in a small neighborhood of that estimate by means of a matrix-multiply DFT. The second registration algorithm registers images using a filtered frequency-domain algorithm based on a computation of the zero-padded FFT[2]. This algorithm is expected to work better when under-sampled or aliased images are considered. Due to the fact that different images have different frequency content and edge information, registration is done on images, gradient images, phase congruency images[4-6], and edge-detected images. Work done by *Boye et al*[3] looked at the registration errors for under-sampled images; however they did not consider the variation of the SNR level.

ANALYSIS AND RESULTS

In determining the registration errors associated with each of the aforementioned registration, we first calculated the signal to noise ratio (SNR) of the noiseless images. The SNR is determined as the ratio of the mean to the standard deviation of each image. A vector of SNR levels is created with the lowest SNR being 10% of the calculated SNR and the highest is two times the SNR of the noise free image.

Several noisy and under-sampled images were created from the ideal noiseless images. Noisy images were then created from ideal images, by adding one of the three types of noises: additive Gaussian noise, fixed-pattern noise along the column direction, and a combination of these two. The Fourier shift theorem is used to perform the lateral shift operation. This theorem states that a lateral shift in the spatial domain is equivalent to a linear phase shift in the frequency domain.

In order to extend the analysis of this paper, the gradient, phase congruency and the edge-detected images were also registered. The interest in the registration of those image metrics is due to the fact that they show edge information and registration of these metric images may improve the registration accuracy.

Once the registrations are done for all the images with the three different additive noise types, a comparison of their registration errors is done to determine which registration technique works better for each of the three images. The three images used to do the analysis are an Air resolution target, an image of the moon, and an aerial image. These original images are shown in Figure 1.

(a) (b) (c)

Figure 1: The noise free images used

A special case of image registration that would be of interest is the registration of the intensity images from an imaging polarimeter, also called a Stokes polarimeter. A Stokes polarimeter is a polarization imaging system that collects several intensity images for different polarization state analyzer orientations. While changing the orientation of the polarization analyzer, one can introduce a shift or rotation in the pixels of the new intensity images. In order to have accurate Stokes parameter information of the light reflected from a scene, it is best to register all the intensity images to each other before calculating the S0, S1, S2, and S3 Stokes parameters. In this analysis we used the DFT registration algorithm to register the intensity images of a Stokes polarimeter.

REGISTRATION OF PROPERLY SAMPLED IMAGES

The images in Figure 2 show the change of the original image in (a) to when the three different types of noises are added, with (b) showing the image with random Gaussian noise, (c) is the image with a fixed pattern noise instead,

and (d) is the combination of both noises. The original image is shifted and then noise added once again to generate a second image which is registered to the first.

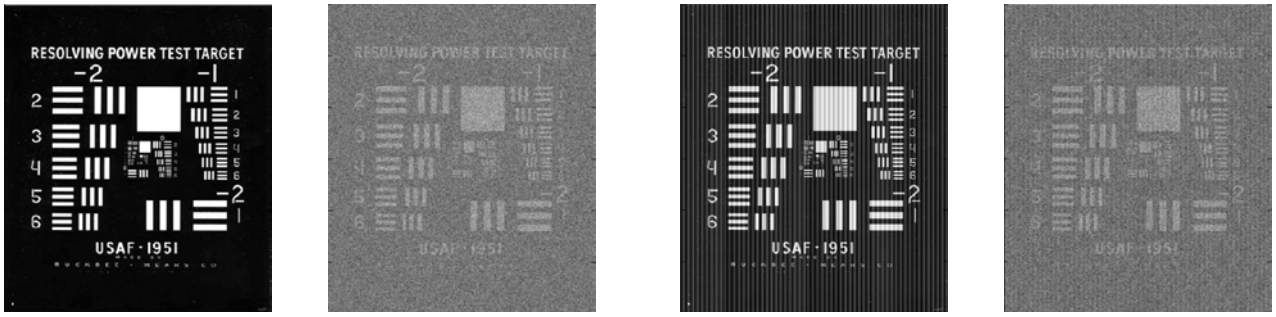

(a) (b) (c) (d)

Figure 2: Image (a) is the original noise free image, (b) is the image with additive random Gaussian noise, (c) is the image with a fixed pattern noise along its column, and (d) is the image with both noises.

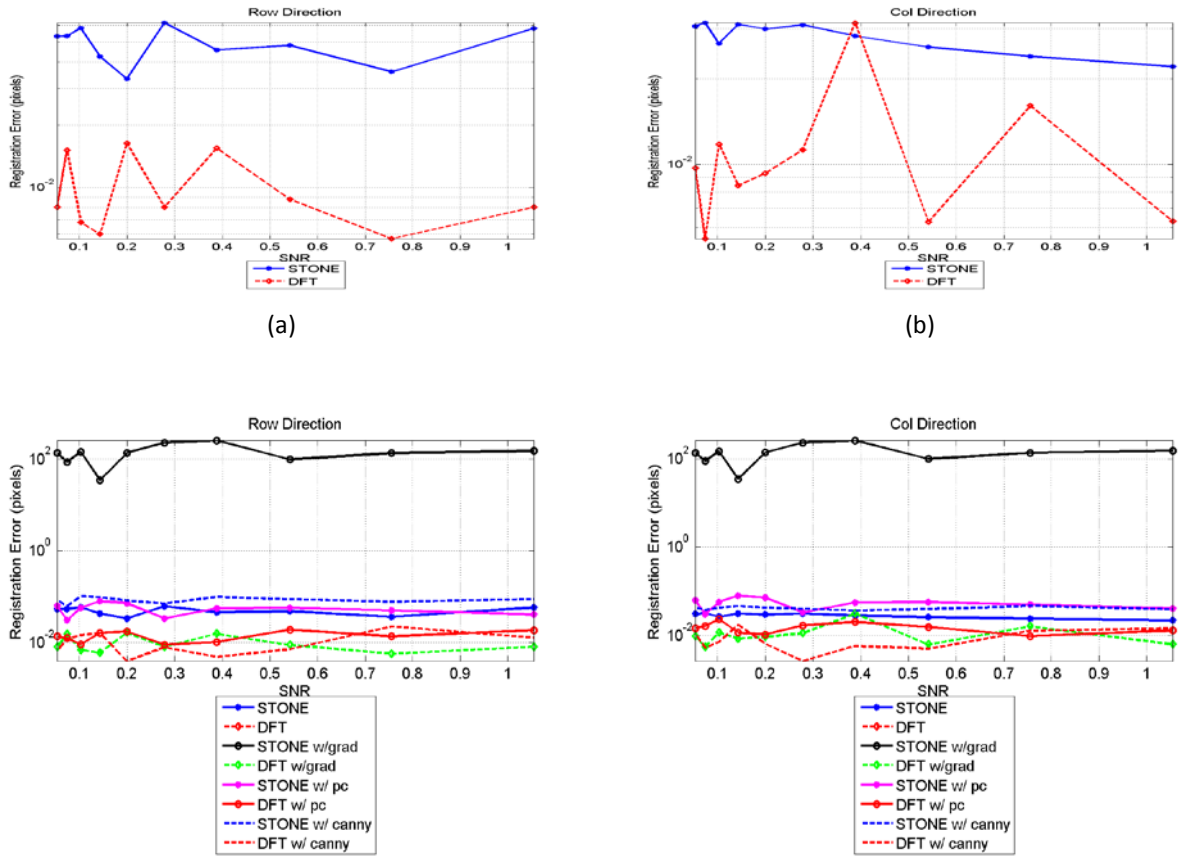

(a) (b)

(c) (d)

Figure 3: Registration error as a function of signal to noise ratio level for the AF1951 resolution target when Gaussian random noise is added. (a) and (c) Show the row direction registration errors while (b) and (d) show the errors in the column direction.

Figure 3 depicts the registration errors for the AF1951 image when random Gaussian noise is added, where (a) and (b) show row and column registration errors for both algorithms when the intensity images are registered; whereas (c) and (d) show the registration errors in the case of registering the images metrics.

The blue and red dashes lines represent the results for registering the Canny edge detected images using the Stone and the DFT algorithms respectively. The black solid line and the green dashed line depict the registration errors of the gradient images registered using the Stone DFT algorithms respectively. The red and magenta solid lines show the results for registration with the phase congruency method using the DFT algorithm and the Stone's algorithm. respectively. Finally, the red dashed line with diamond shapes shows the results of DFT registration algorithm on intensity images, and the blue solid line is the result of registration with Stone's method. This color coding of the plotted data holds throughout the entire paper.

By adding a random Gaussian noise to the AF1951 image, the image contrast decreased but the shape of the bars in the image are still visible; however the shape of the letters were significantly deteriorated. Figure 3 shows that the DFT registration worked well for all the images, but it worked best when registering the metric images instead of the intensity image. Since the edges are still visible in the noisy images, calculating the gradient or the Canny edge detection will help maximize the registration accuracy. Instead of locating edges, the phase congruency method looks at regions in the image where there is a high change in phase. Registering phase congruency images also improved the registration accuracy. Stone's algorithm failed when the gradient images were registered.

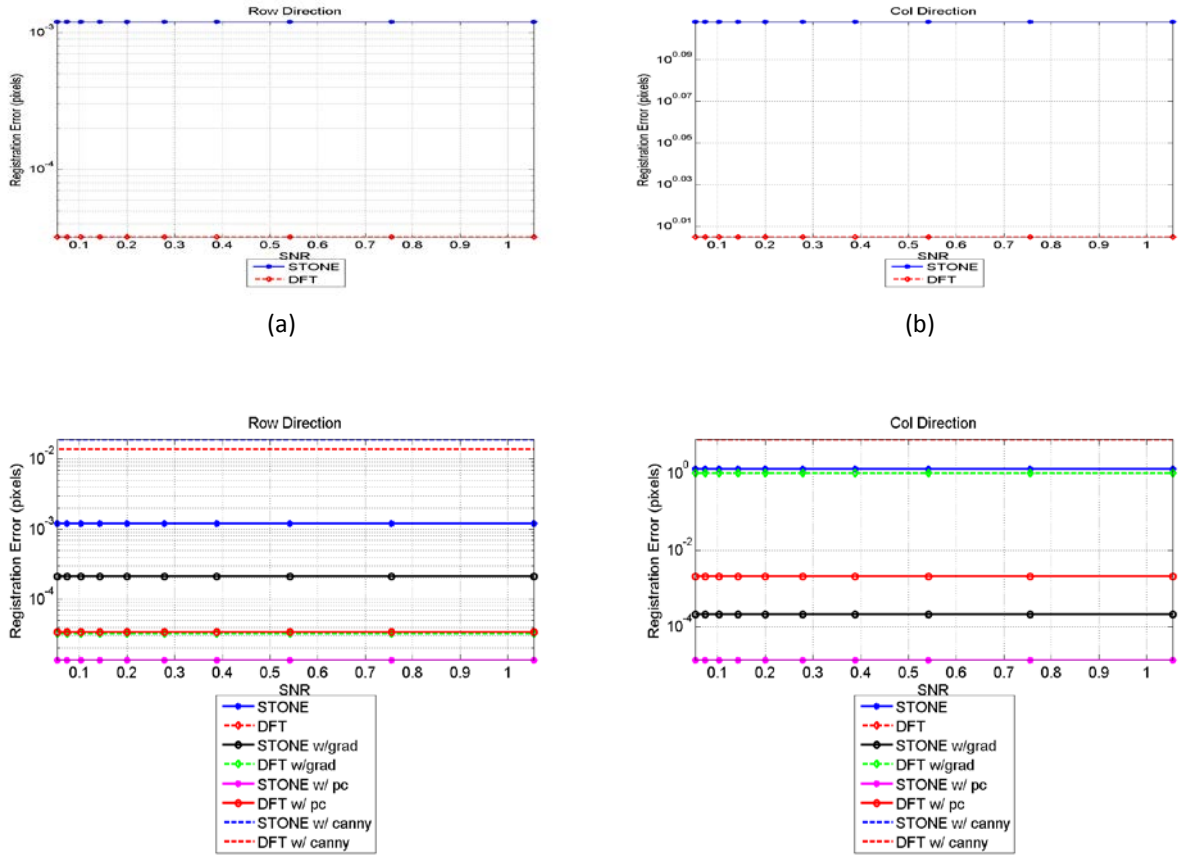

Figure 4: Registration error as a function of signal to noise ratio level for the AF1951 test target when a fixed pattern noise is added to its column.(a) and (c) Show the row direction registration errors and (b) and (d) show the ones in the column direction.

As the lines created by the fixed pattern noise distorted most of the vertical lines in the images, this effect lead to the failure of the registration algorithms when the intensity images are registered, as shown in Figure 4-(b). The registration algorithms worked well with all the other metric images as the bar edges still going to show clearly and the phase shift between the black and white regions are also preserved.

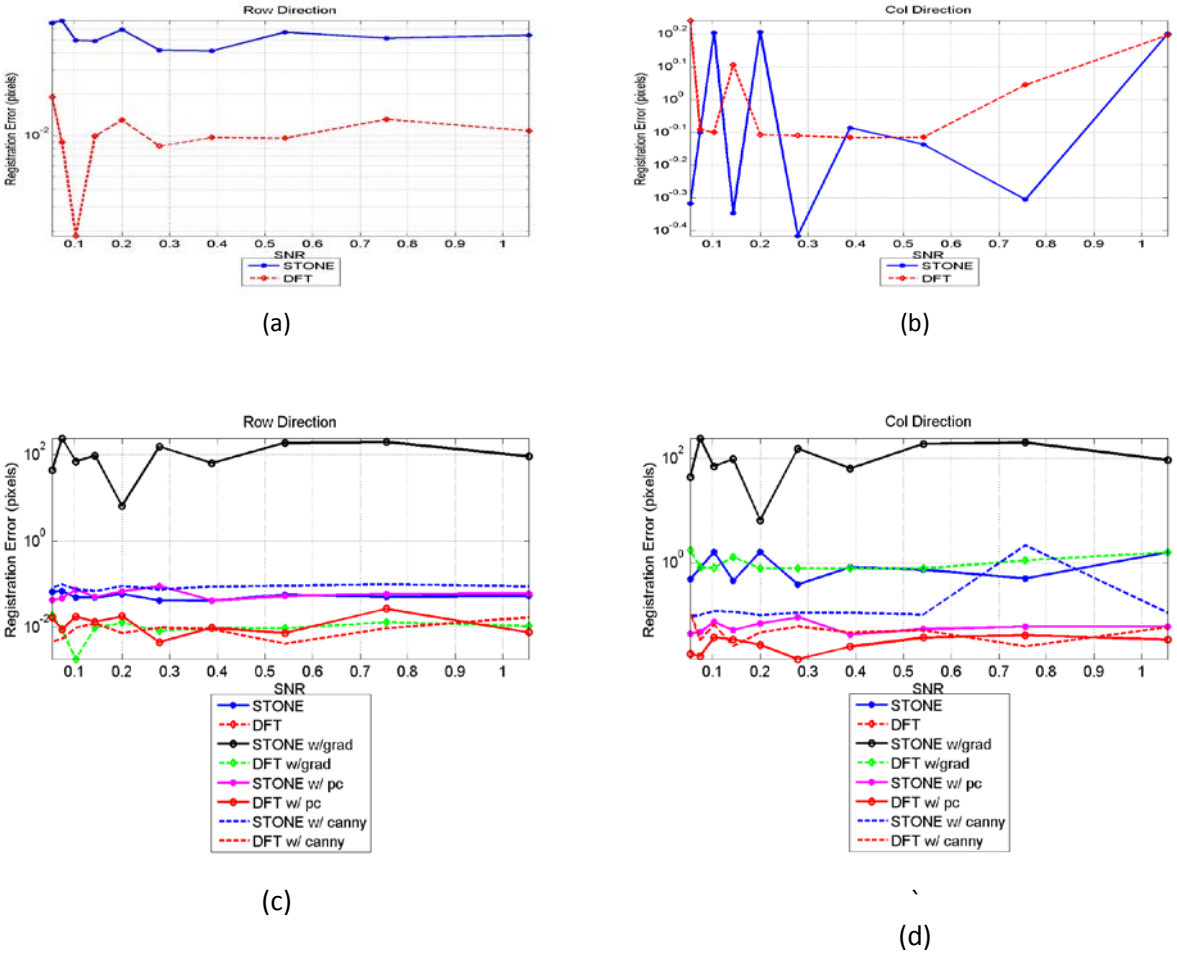

Figure 5: Registration error as a function of signal to noise ratio level for the AF1951 test target when both a Gaussian random noise and a fixed pattern noise are added.(a) and (c) Show the row direction registration errors and (b) and (d) show the ones in the column direction.

The results of Figure 5 also show the same outcome as in the case of only Gaussian noise is present. However in this case the Stone's method failed when registering the intensity images as well as when registering the gradient of the images.

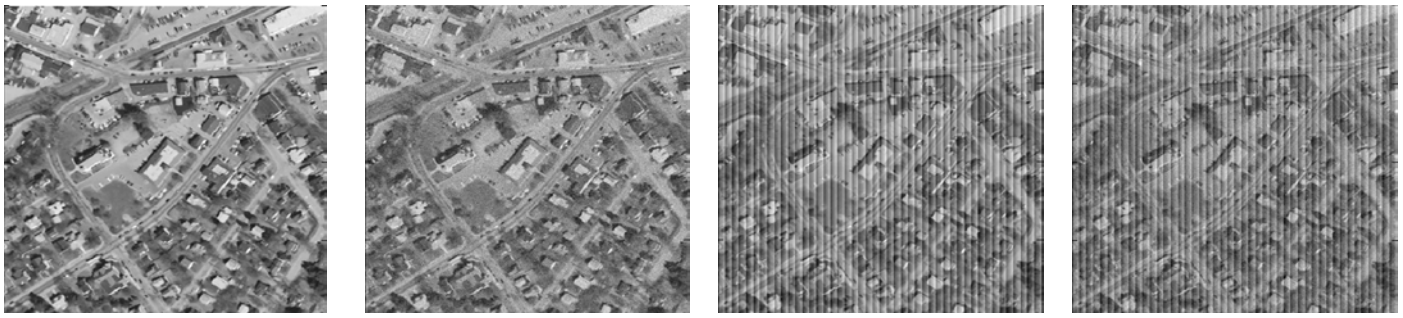

(a) (b) (c) (d)

Figure 6: The aerial image and its noisy version. (a) Shows the original image, (b) is the image with a random Gaussian added to it, (c) is the image with a fixed patterned noise added to its column, and (d) is the image with both noises added.

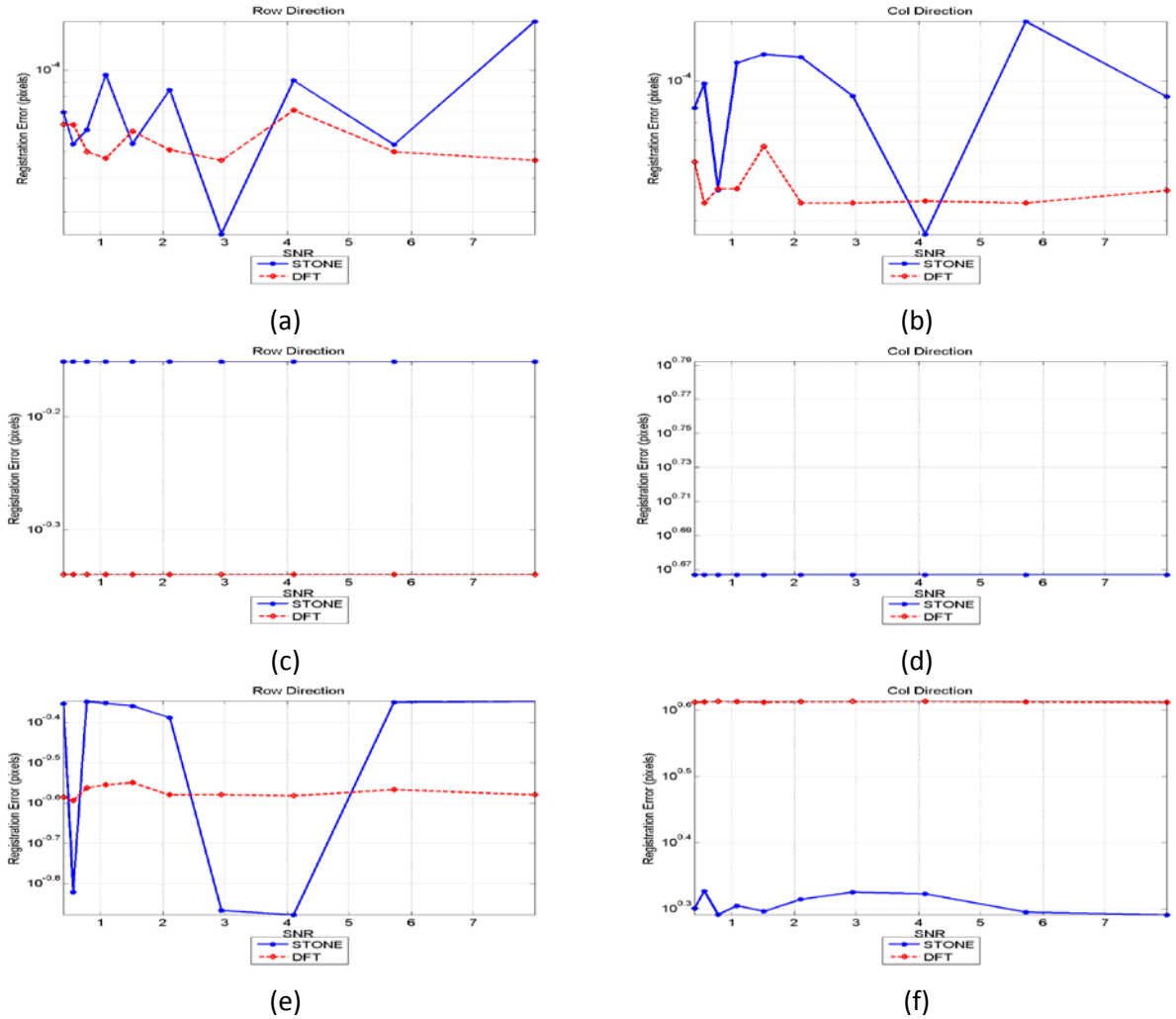

Figure 7: Registration error vs SNR for intensity registration with both algorithms. Figure 7 (a) and (b) are the errors for the case when a random Gaussian noise is added, and (c) and (d) are for when a fixed pattern noise is added, and (e) and (f) show the results for the case when both noises are present.

In the case of this particular image, the addition of the fixed pattern noise did not affect the intensity registrations with both algorithms; however the fixed pattern noise completely changed the images, and led both algorithms to fail.

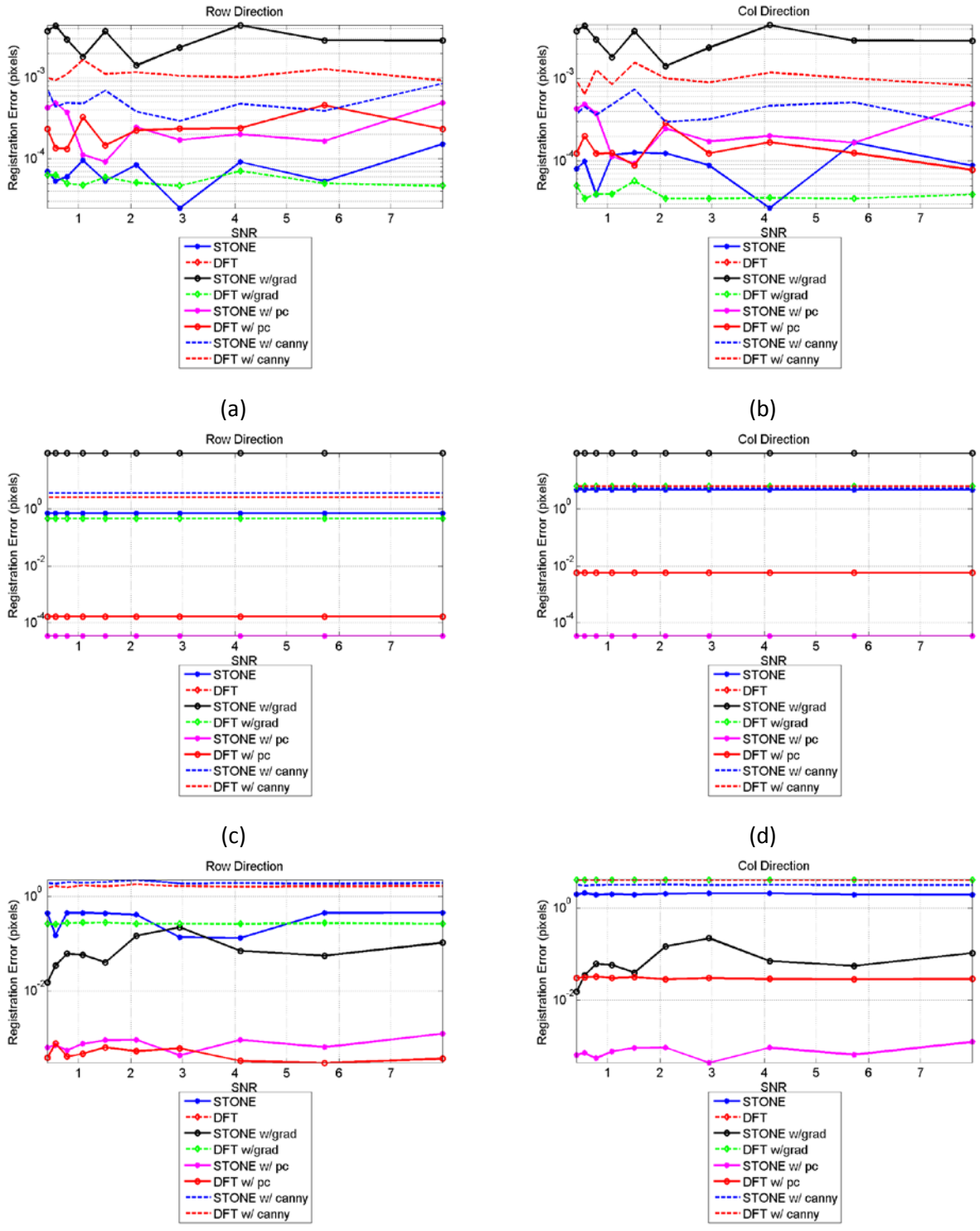

Figure 8: Registration error vs SNR for the aerial image. (a) and (b) show the results for the case when only random Gaussian noise is added, (c) and (d) show the results for the case when a fixed patterned noise is added to the column of the image, and (e) and (f) depict the results for when both noises are present.

Furthermore, when registrations are performed on the other images, all algorithms succeed for the case of the Gaussian noise, as depicted by Figure 8. But in the presence of a fixed pattern noise then the phase congruency method is the only metric image that worked well. The main reason that the Gaussian noise did not affect the registration process is because the presence of the noise did not change the patterns in the image, whereas the fixed pattern noise destroyed some patterns in the image, making the matching of the features harder.

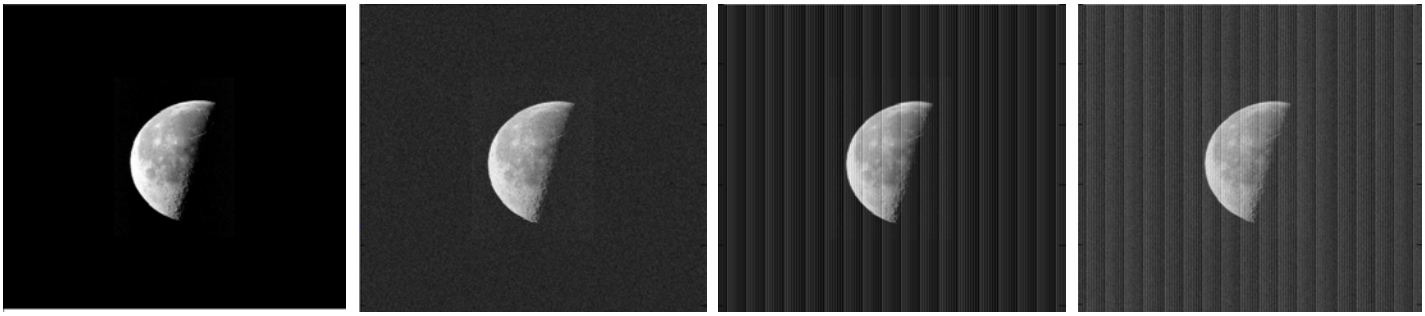

Figure 9: The image of the moon and its noisy version. (a) Shows the original image, (b) is the image with a random Gaussian added to it, (c) is the image with a fixed patterned noise added to its column, and (d) is the image with both noises added.

As for the image of the moon, the moon itself is brighter than every other region of the image, even after the addition of the random Gaussian. Thus both algorithms registered the intensity image with little error, as shown in figure 10 (a) and (b). However when the fixed pattern noise is added then the registrations start to fail in the column direction; moreover when both noise terms are added, Stone's algorithm improved slightly.

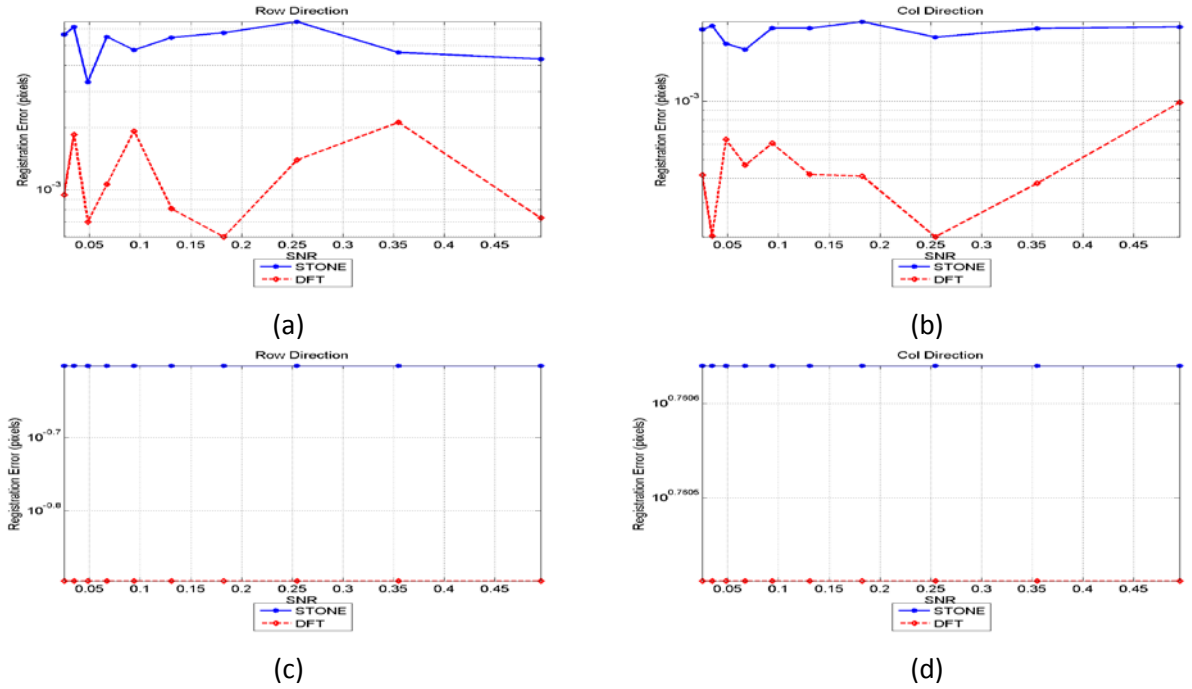

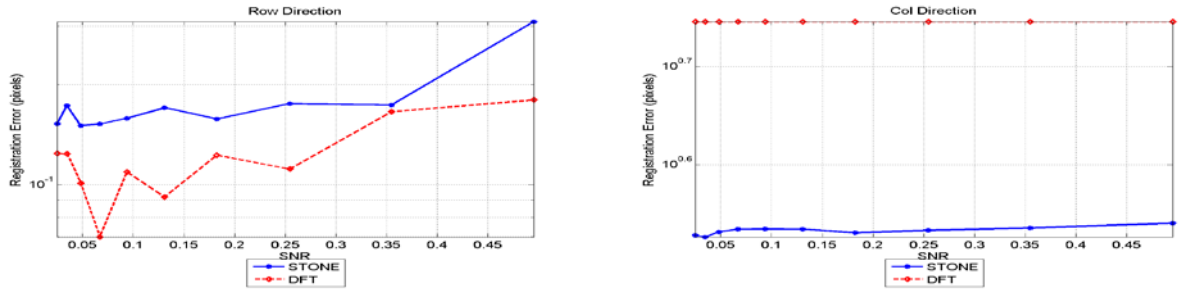

(e) (f)

Figure 10: Registration error vs SNR for the intensity image of the moon is registered using both algorithms. Figure 10 (a) and (b) are the errors for the case when a random Gaussian noise is added, and (c) and (d) are for when a fixed pattern noise is added, and (e) and (f) show the results for the case when both noises are present.

Again unless the amount of Gaussian is more than 50% of the maximum value in the image, the brightness of the moon is going to always exceed its surrounding; thus both algorithms are going the work well with all the metric images as well, and the results of these registrations are shown in Figure 11 (a) and (b). For example with the phase congruency method, the registration worked better than all other methods because the high phase change in the image is at the contours of the moon. Then when the gradient of the canny edge detection of the images are calculated, the contour of the moon get traced very nicely, leaving a perfect region to register. In the presence of the fixed pattern noise, only the phase congruency registration succeeded with both algorithms, and that is because of the phase change at the contour of the moon. The gradient and the canny edge detection will emphasize the vertical lines of the fixed pattern noise, thereby decreasing registration accuracy.

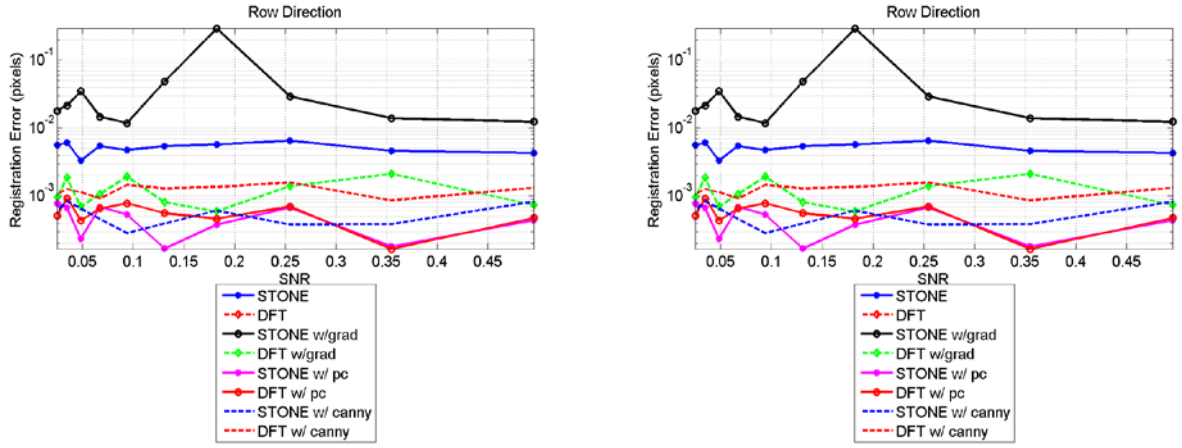

(a) (b)

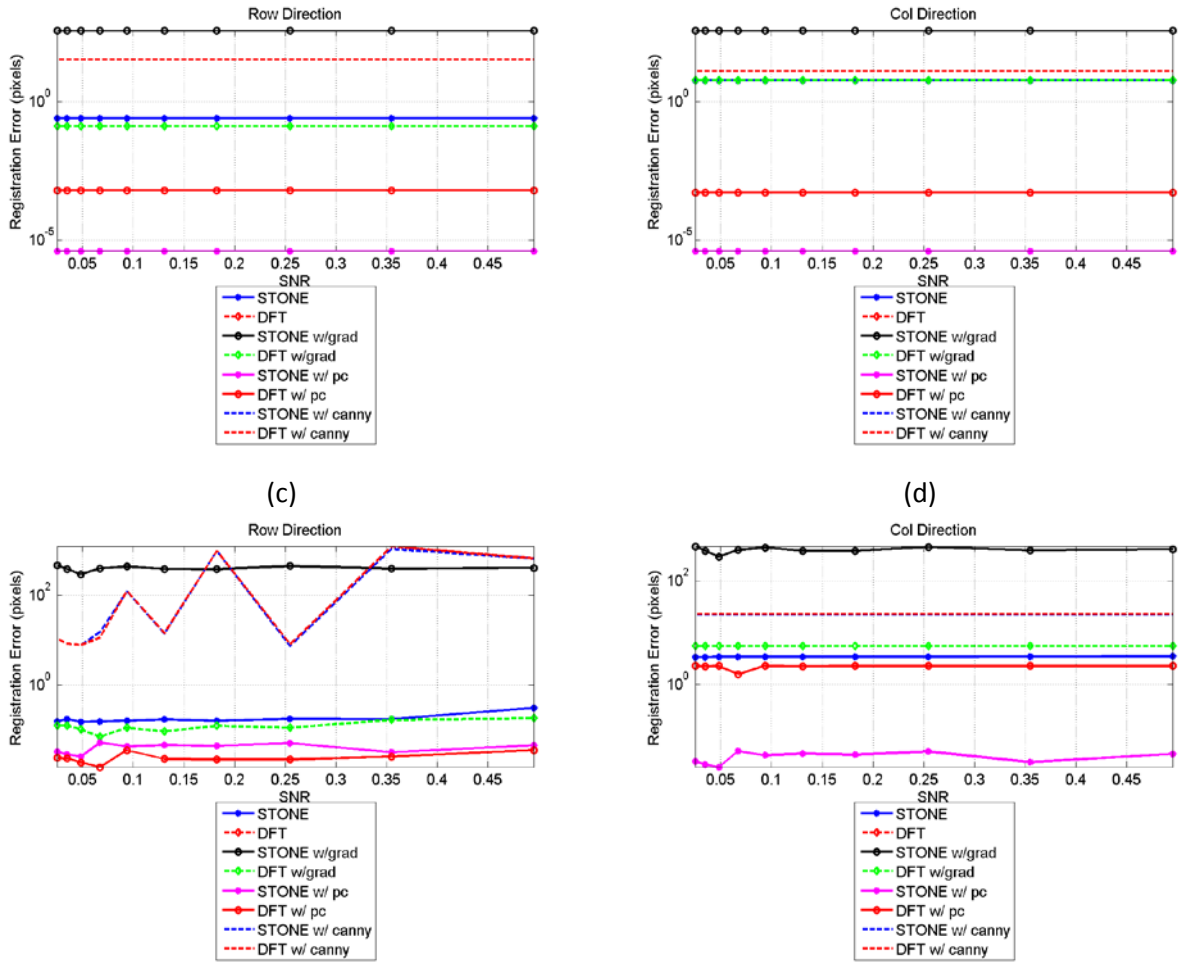

Figure 11: Registration error vs SNR for the metric images of the moon. (a) and (b) show the results for the case when only random Gaussian noise is added, (c) and (d) show the results for the case when a fixed patterned noise is added to the column of the image, and (e) and (f) depict the results for when both noises are present.

UNDER-SAMPLED IMAGES

In this section we investigate the registration of under-sampled images in the presence of noise. The signal-to-noise ratio level is also considered. All under-sampled images are registered using the DFT algorithm and Stone's algorithm.

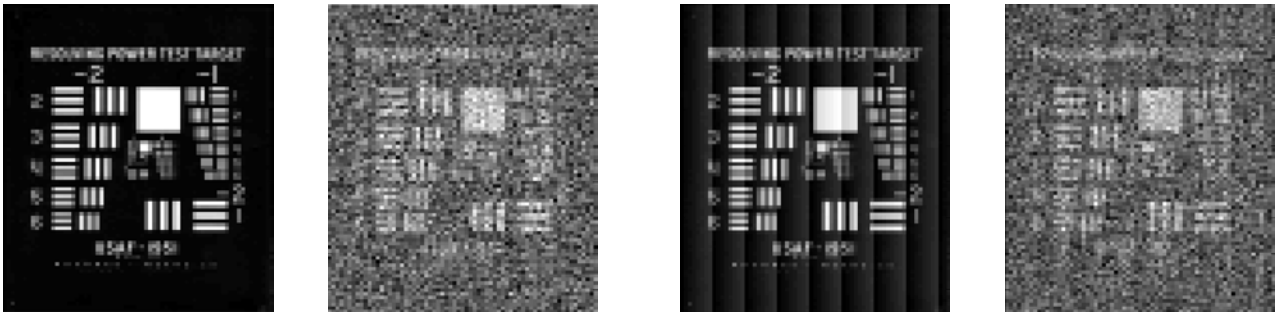

(a) (b) (c) (d)

Figure 12: Images of the under-sampled AF1951 with additive noise. (a) Is the original under-sampled image, (b) Shows the under-sampled image with random Gaussian noise, (c) is the case when a fixed pattern noise is added to the image, and (d) is the case with both noises present.

Figure 12 shows images of the under-sampled AF1951 resolution target along with associated noisy images. Clearly significant information is lost in the under-sampled and noisy images. This is expected to reduce registration accuracy. Figure 13 shows in (a) - (d) that both algorithms failed at very low SNR; however Stone's algorithm on the intensity image and the DFT algorithm on the gradient image recovered very quickly as the level of SNR was increased. When the fixed pattern noise was added to the images all algorithms registered with very small errors.

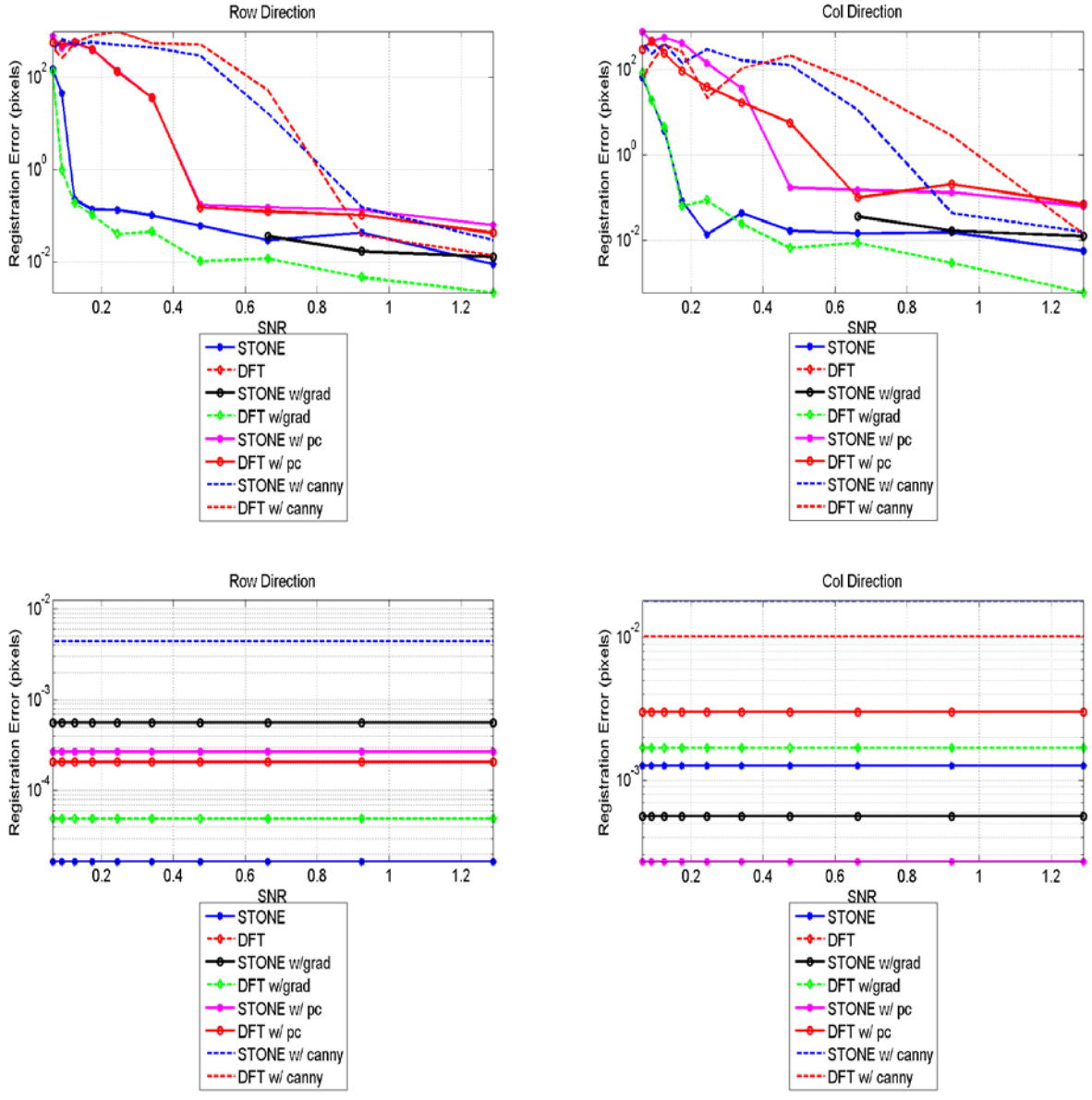

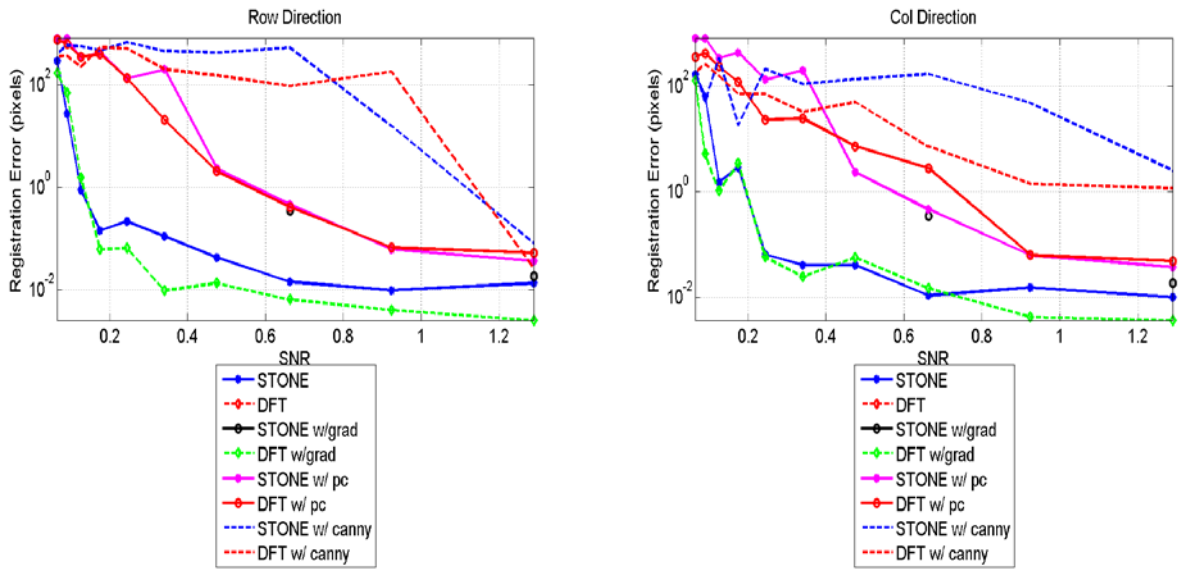

Figure 13: Registration error vs SNR for the metric images of the moon. (a) and (b) show the results for the case when only random Gaussian noise is added, (c) and (d) show the results for the case when a fixed patterned noise is added to the column of the image, and (e) and (f) depict the results for when both noise terms are present.

REGISTRATION OF INTENSITY IMAGES FROM A STOKES POLARIMETER

In this section we demonstrate the use of the DFT registration algorithm to register the intensity images from a Stokes polarimeter. We reconstruct the S1 and S2 Stokes images along with the degree of linear polarization (DoLP) and compare them to when the images were not registered. Figure 14 shows the polarization data obtained before registration of the images and figure 15 shows the data after registration.

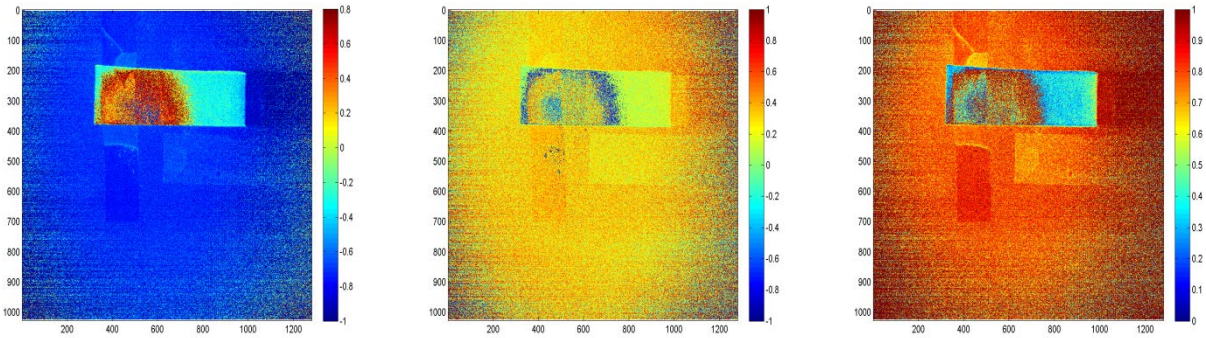

(a) (b) (c)

Figure 14: Polarization data before registration, where (a) is the S1 element of the Stokes vector, (b) is S2 element of the Stokes vector, and (c) is the DoLP image.

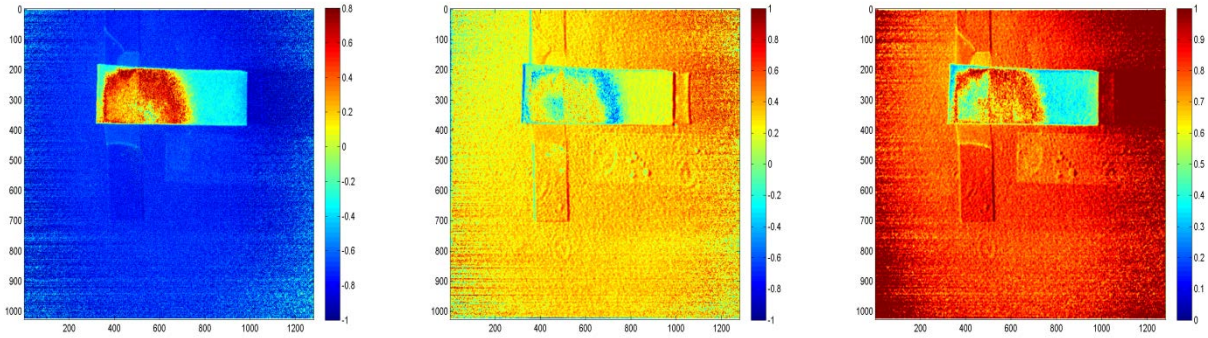

(a) (b) (c)

Figure 15: Polarization data after registration, where (a) is the S1 element of the Stokes vector, (b) is S2 element of the Stokes vector, and (c) is the DoLP image.

By comparing the images of Figures 14 and 15 to each other, we notice that the polarization maps are similar. However the image quality is much better when the intensity images are registered before processing. For example, the edge features are much clearer in the images of Figure 15, which show more information that one could not see in images of Figure 14. This process could be used for Mueller matrix polarimetry as well.

CONCLUSION

In this work we have presented the registration error of two different registration algorithms. Registration errors were investigated for three different images. Registration was performed on properly sample images and under-sampled images as well. We also performed the registration on the gradients of the images, the phase congruency images, and the edge-detected images. It was determined from the results that Stone's method performed better when registering images, and was best in the case of under-sampled images. The DFT algorithm's performance varied depending on the frequency, phase, and edge contents of the images. Both registration algorithms were not affected by Gaussian noise unless the noise level was high enough to wash out the image features. However, even a very low level of fixed pattern noise tends to lead both algorithms to fail by an order of magnitude at least. Registration of the phase congruency, gradient, and edge-detection images were determined to be the best choices.

ACKNOWLEDGEMENTS:

Sandia is a multiprogram laboratory operated by Sandia Corporation, a Lockheed Martin Company, for the United States Department of Energy's National Nuclear Security Administration under contract DE-AC04-94AL85000.

REFERENCES

[1]. M. G. Sicairos, S. T. Thurman, and J. R. Fienup, "Efficient subpixel image registration algorithms," Opt. Lett. Vol. 33, No. 2, 156-158 (2008).

[2]. J.R. Fienup and A.M. Kowalczyk, "Phase retrieval for a complex-valued object by using a low-resolution image," J. Opt. Soc. Am. A 7, 450-458(1990).

[3]. H. S. Stone, M. T. Orchard, C. Chang, and S. A. Martucci, "A Fast Direct Fourier-Based Algorithm for subpixel Registration of Images," IEEE, Vol. 39, No. 10, 2235-2243 (2001).

[4]. M. G. Sicairos, S. T. Thurman, and J. R. Fienup, “Efficient subpixel image registration algorithms,” Opt. Lett. Vol. 33, No. 2, 156-158 (2008).

[5]. H. S. Stone, M. T. Orchard, C. Chang, and S. A. Martucci, “A Fast Direct Fourier-Based Algorithm for subpixel Registration of Images,” IEEE, Vol. 39, No. 10, 2235-2243 (2001).

[6]. R. R. Boye, and C. L. Nelson, “Comparison of Subpixel Image Registration Algorithms,” Pro. SPIE 7246, 72460X-1-8 (2009).

[7]. P. D. Kovesi, “Image features from phase congruency,” Videre: Journal of Computer Vision Research 1 (1999) 1-26 http://mitpress.mit.edu/e-journals/Videre/.

[8]. P. D. Kovesi, “Phase Congruency Detects Corners and Edges,”

[9]. P.D. Kovesi, Phase congruency: A low-level image invariant. Psychological Research 64 (2000) 136-148

[10]. D. H. Goldstein, *Polarized Light,* (CRC Press, Boca Raton, Third Edition)